

Site-Directed Mutagenesis at the MoCo Site of the Human Aldehyde Oxidase: Interrogating the Kinetic Differences Between Human and Cynomolgus Monkey

Armina Abbasi, Carolyn A. Joswig-Jones,
and Jeffrey P. Jones

Department of Chemistry, Washington State University, Pullman, WA 99164-4630

Running title: Kinetic differences between human and cynomolgus monkey aldehyde oxidase.

Corresponding author: Jeffrey P. Jones, Ph.D.

Department of Chemistry

Washington State University

Pullman, WA 99164-4630

Tel: +1(509) 592-8790

E-mail: jjp@wsu.edu

Number of pages: 35

Number of Figures: 4

Number of Tables: 3

Number of references: 45

Number of words in Abstract: **249**

Number of words in Introduction: **736**

Number of words in Discussion: **1233**

Abbreviations: ADNTN, aminodantrolene; AIC, Akaike information criterion; AO, aldehyde oxidase; AOX, aldehyde oxidase gene; CYP450, cytochrome P450; DMSO, dimethyl sulfoxide; EDTA, ethylenediaminetetraacetic acid; FAD, flavin adenine dinucleotide; **hAO**, purified expressed human aldehyde oxidase; K_m , Michaelis-Menten constant; MAM, modified activity model; **mAo**, purified expressed cynomolgus monkey aldehyde oxidase 1; MoCo, molybdenum

pterin cofactor; O6BG, O⁶-benzylguanine; OAR, [8-oxo-benzylguanine] to [aminodantrolene] ratio; TDI, time-dependent inhibitor; LC-MS/MS, liquid chromatography-tandem mass spectrometry.

Abstract:

The estimation of the drug clearance by aldehyde oxidase (AO) has been complicated because of this enzyme's atypical kinetics and species and substrate specificity. Since humans (**hAO**) and cynomolgus monkeys (**mAO**) have a 95.1% sequence identity, cynomolgus monkeys may be the best species for estimating AO clearance in humans. Here, O⁶-benzylguanine (O6BG) and dantrolene were used under anaerobic conditions, as oxidative and reductive substrates of AO respectively, to compare and contrast the kinetics of these two species through numerical modeling. While dantrolene reduction followed the same linear kinetics in both species, the oxidation rate of O6BG was also linear in mAO and did not follow the already established biphasic kinetics of hAO. In an attempt to determine why hAO and mAO are kinetically distinct, we have altered the hAO V811 and F885 amino acids at the oxidation site adjacent to the molybdenum pterin cofactor (MoCo) to the corresponding alanine and leucine in mAO respectively. Although some shift to a more monkey-like kinetics was observed for the V811A mutant, six more mutations around the AO cofactors still need to be investigated for this purpose. In comparing the oxidative and reductive rates of metabolism under anaerobic conditions, we have come to the conclusion that despite having similar rates of reduction (4-fold difference), the oxidation rate in mAO is more than 50-fold slower than hAO. This finding implies that the presence of nonlinearity in AO kinetics is dependent upon the degree of imbalance between the rates of oxidation and reduction in this enzyme.

Significance Statement:

Even with having as much as 95.1% sequence identity, human and cynomolgus monkey aldehyde oxidase are kinetically distinct. Therefore, monkeys may not be good estimators of drug clearance in humans.

Introduction:

Aldehyde oxidase (AO) is a molybdoflavoprotein mostly found in three different oligomeric states as a 150 kDa monomer, a homodimer, and a tetramer (Mendel, 2009; Mota *et al.*, 2019). In recent years, efforts to make drugs less susceptible to metabolism by CYP450 family of enzymes, which act via electrophilic attack, have led to an increase in substrates with a higher susceptibility to AO metabolism, which occurs via nucleophilic attack. (Dowers *et al.*, 2004; Alfaro *et al.*, 2008; Pryde *et al.*, 2010; Davydova *et al.*, 2019).

AO is capable of oxidation of a wide range of compounds such as aldehydes, alicyclic iminium ions and aromatic azaheterocycles (Pryde *et al.*, 2010) and the oxidation half-reaction is believed to occur close to the MoCo site (Coelho *et al.*, 2015). Molecular oxygen is assumed to be the final electron acceptor in the AO catalytic cycle (Alfaro *et al.*, 2008; Pryde *et al.*, 2010). Until recently it was believed that reduction of other substrates, such as the ones containing nitro groups, by AO would only happen under anaerobic conditions (Li *et al.*, 2009; Weidert *et al.*, 2013; Maia *et al.*, 2015). However, quite a few examples of aerobic nitro reduction have been presented in the literature in the past few years (Konishi *et al.*, 2017; Amano *et al.*, 2018; Ogiso *et al.*, 2018). This has in turn brought up the possibility of a competition between the reductive substrates and the molecular oxygen at the FAD site (Paragas *et al.*, 2017a).

Many promising drug candidates are removed from the pipeline or are chemically modified due to poor estimation of their metabolism by AO in humans, examples include BIBX1382 (Dittrich *et al.*, 2002), SGX523 (Diamond *et al.*, 2010) and RO1 (Zhang *et al.*, 2011). One commonly used preclinical method for estimation of drug clearance in humans is the use of interspecies allometric scaling (Nair *et al.*, 2016). However, this approach, which is based on scaling by weight, is limited as it ignores several factors such as protein binding, physicochemical

properties of the drug, and interspecies differences in metabolism and transport (Sharma *et al.*, 2009). Despite efforts to incorporate these absorption, distribution, metabolism, and excretion (ADME) parameters into a single animal model for estimation of AO clearance in humans, trends observed to date have not been generalizable. Consequently, alternative methods such as in vitro scaling or multiple species allometry have been suggested for this enzyme (Zientek *et al.*, 2010; Crouch *et al.*, 2018). The complicated interspecies differences for AO may have arisen due to the presence of various isoforms in different species or the multiple active sites present in this enzyme (Hoshino *et al.*, 2007; Garattini *et al.*, 2009; Paragas *et al.*, 2017a)

The number of AOX active genes in traditional preclinical species varies from none in dogs hepatocytes to the extreme of four in rodents (Garattini *et al.*, 2009). When more than one AO isozyme is present in a species, they typically exhibit tissue specificity (Cheshmazar *et al.*, 2019). In humans, only the AOX1 gene shows activity and the other two pseudogenes (AOX2 and AOX4) remain inactive despite being transcribed. The same trend is observed in chimpanzees, demonstrating that this functional inactivation of AOX4 and AOX2 occurred before the human speciation occurred (Garattini *et al.*, 2009; Cheshmazar *et al.*, 2019). Depending on the substrate, various species exhibit different levels of activity. For example, rabbit metabolizes methotrexate and cinchonidine several orders of magnitude faster than rhesus monkey, and monkey is faster than human (Itoh *et al.*, 2006b; Choughule *et al.*, 2015). Alternatively, a rank order of rabbit, human, monkey was assigned to zoniporide (Dalvie *et al.*, 2013). Furthermore, studies on several other substrates such as zonisamide, (S)-RS-8359, phthalazine, and DACA have observed the highest AO activity in monkeys and humans, followed by rabbits, guinea pigs and rodents (Itoh *et al.*, 2006a; Fukiya *et al.*, 2010; Choughule

et al., 2013). To learn more about AO species differences, we sought to understand whether specific amino acids at the oxidation active site in humans and nonhuman primates were contributing to the divergent activities observed. Cynomolgus monkeys share a 95.1% AO amino acid sequence identity with humans, and their small size makes this a species of high interest (Hoshino *et al.*, 2007). Furthermore, cynomolgus monkeys were selected for this study based on their recently reported promising and comparable intrinsic clearance with human for BIBX1382 (Hutzler *et al.*, 2014) which has been in agreement with several earlier studies (Kawashima *et al.*, 1999; Itoh *et al.*, 2006b; Diamond *et al.*, 2010; Garattini *et al.*, 2012).

Numerical fitting of kinetic profiles allows for flexibility in data analysis and an enhanced understanding of kinetic mechanisms. Kinetic modeling is the method of choice over the analytical Michaelis-Menten method to study enzymes with atypical kinetics such as AO. Traditional kinetic methods rely on several assumptions such as the steady state hypothesis that limits and occasionally misdirects our understanding of the kinetic data. Based on our previous studies on the human aldehyde oxidase (hAO), we have found that this enzyme shows a nonlinear behavior and should be assessed numerically to take the whole kinetic process into account instead of truncating the data to meet the Michaelis-Menten assumptions (Abbasi *et al.*, 2019). Here, we use the same numerical approach to investigate the basis of interspecies kinetic differences between human and cynomolgus monkey.

Materials and Methods

Chemicals and Reagents

O⁶-benzylguanine (O6BG) and its metabolite, 8-oxo-benzylguanine were purchased from Toronto Research Chemicals (North York, ON). Dantrolene was purchased from Cayman Chemical Company (Ann Arbor, MI) and the metabolite, aminodantrolene (ADNTN), was synthesized as described elsewhere (Amano *et al.*, 2018). Phenacetin, glucose oxidase (*Aspergillus* spp.), glucose, and catalase (bovine liver) were purchased from Sigma-Aldrich (St. Louis, MO). The monobasic potassium phosphate, dibasic potassium phosphate, and EDTA used for the potassium phosphate buffer were purchased from JT Baker (Center Valley, PA).

Site-Directed Mutagenesis and cDNA Analysis

The QuikChange® II site-directed mutagenesis kit from Agilent (Santa Clara, CA) was used to make the single and double mutants on the codon-optimized pTHco-hAOX1 plasmid (Foti *et al.*, 2016). The primers (Table 1) for this study were designed through the Agilent's QuikChange primer design platform and bought from Invitrogen. The resulting PCR products from following the QuikChange mutagenesis protocol were purified using the Wizard® plus midiprep DNA purification system. The sequence analysis was performed using a 3730 DNA Analyzer and the BigDye Terminator ready reaction mix from Applied Biosystems. A Blast sequence alignment was performed to confirm the mutations. To make the FLVA double mutant, the purified F885L plasmid was used as the DNA template to be mutated once more with the primers designed to incorporate the V811A mutation.

*Expression of AO in *E. coli**

Expression and purification of human aldehyde oxidase (**hAO**) was performed according to the method previously described (Alfaro *et al.*, 2009; Paragas *et al.*, 2017b). The cynomolgus monkey aldehyde oxidase (**mAO**) plasmid was a gift from Professor Yori-hisa Tanaka (Hoshino *et al.*, 2007). The expression and purification process of **mAO** as well as of the three mutants was similar to that of **hAO**. The total amount of the purified enzyme was quantified by liquid-chromatography-tandem mass spectrometry (LC-MS/MS) (Barr *et al.*, 2013b).

Time Course Kinetic Assays

All the assays were done under anaerobic conditions: 30 units/mL final concentration of glucose oxidase and 150 units/mL of catalase were added to each reaction vial containing saturating amounts (5 times the K_m) of O6BG (200 μ M) and dantrolene (30 μ M) dissolved in 0.1M potassium phosphate buffer (**pH** 7.4) containing 0.1mM EDTA. Next, 50 mM of glucose was added to each incubation after they were prewarmed for 5 minutes at 37°C to start the depletion of the molecular oxygen in the reaction. The biotransformation would then be initiated after 5 minutes by adding 1 μ l of the purified enzyme. The final AO concentration for **hAO**, **mAO**, F885L, V811M and FLVA was 38.4 nM, 10.1 nM, 28.6 nM, 45.0 nM and 46.3 nM respectively. The total reaction volume was 1.5 mL and 100 μ L of it was quenched at 0.2, 3, 10, 20, 30, 45, 60, 90, and 120 minutes in 25 μ L of 1M formic acid containing 10 μ M phenacetin as an internal standard. The enzyme assays were all done in triplicates and the goodness of fit was evaluated using the R squared and Akaike Information Criteria (AIC) values.

Liquid Chromatography- Mass Spectrometry

Samples were analyzed using an LC-20AD series high-performance LC system (Shimadzu, Columbia, MD) fitted with an HTC PAL autosampler (LEAP Technologies, Carrboro, NC). Chromatography was performed using a Kinetex® 2.6 μm C18 100 Å column (100 \times 2.1 mm; Phenomenex). Mobile phase A consisted of 0.05% (by volume) formic acid and 0.2% acetic acid (MilliporeSigma, Billerica, MA) in water, and mobile phase B comprised 90% acetonitrile (MilliporeSigma), 9.9% water, and 0.1% formic acid (Fischer Scientific, Pittsburgh, PA). The quantitation was conducted on an API 4000 Q-Trap MS system (Applied Biosystems/MDS Sciex, Foster City, CA) with turbo spray electrospray ionization operating in positive ion mode. The chromatography for all the analytes started at 10% mobile B concentration and would ramp up to 75% mobile B in 6 minutes and the concentration was maintained for half a minute before ramping back down to 10% mobile B in one minute. The MS tuning parameters used were as follows: curtain gas, 20; ion spray voltage, 4900; desolvation temperature, 600°C; ion source gas 1, 35; ion source gas 2, 55; collision gas, medium; declustering potential, 70; entrance potential, 10; collision energy, 35; cell exit potential, 15. The flow rate was 0.25 mL/min and the metabolites and internal standard were detected using multiple reaction monitoring mode following these m/z transitions: 8-oxo-benzylguanine, 258.2 \rightarrow 91.0; ADNTN, 285.1 \rightarrow 186.0 and phenacetin (internal standard), 180.2 \rightarrow 110.1.

Data Analysis

Numerical fitting in Mathematica 11.0.1.0 (Wolfram Research, Champaign, IL) was performed using the NDSolve function with MaxSteps \rightarrow 10000 and PrecisionGoal \rightarrow ∞ ; k_1 was fixed to 270 $\mu\text{M s}^{-1}$ and k_2 was set to $k_1 \times K_m$ for each substrate. The K_m for each substrate was derived from the data on file and was set to 70 μM for O6BG in **hAO**, 7 μM in **mAO**, and 10 μM for the

mutants. For dantrolene, the K_m was set to 5 μM for all the enzyme sources. Model fitting was done using the NonlinearModelFit function with 1/Y weighting. The goodness of fit was evaluated by AIC and RSquared commands. The models used were the Modified Activity Model (MAM) and the linear (Michaelis-Menten) model as described previously (Abbasi *et al.*, 2019). The decision on what model to choose for each dataset was made by comparing the Akaike values (AIC) obtained through the fits to each model.

Results

Kinetic modeling

Here, we used a kinetic modeling approach to determine the rate of oxidation and reduction half-reactions for AO. For the oxidation half-reaction, we used O6BG as a substrate. Oxygen is a challenging substrate to probe. Therefore, to remove any complexities raised by competition between the reductive substrates, we substituted oxygen with dantrolene as a reducing substrate of AO under anaerobic conditions to probe the reduction half-reaction in this enzyme (Amano *et al.*, 2018) as described in the methods section. We chose dantrolene as the reducing substrate in this study based on the previous reports of this compound being metabolized by AO even under normal oxygen concentration as well as its lack of competition with oxidative substrates and having a high turn-over rate among other structurally similar reductive substrates of AO (Amano *et al.*, 2018; Ogiso *et al.*, 2018). Furthermore, dantrolene has a similar K_m to oxygen with the K_m of oxygen for hAO being estimated to be close to 2 μM (Abbasi *et al.*, 2019) and the K_m of dantrolene being 5 μM (data not shown).

Analysis of 8-oxo-O6BG formation over time demonstrates that while hAO has biphasic kinetics, mAO is linear (Fig. 1-A, B). The MAM model was used to account for the curvature in the rate of 8-oxo-O6BG formation in hAO. Numerical fitting to MAM solves for the unknown rate constants k_{3_ox} and k_5 in the model with k_{3_ox} representing the initial fast oxidation rate in hAO and k_5 representing the turn-over rate during the second phase of catalysis where reduction is assumed to be the rate-limiting step (Figure 1A- kinetic scheme inset). It is important to note that k_5 is used to represent the rate of reduction and/or the rate of enzyme re-oxidation interchangeably throughout this paper. This biphasic kinetic behavior does not exist for O6BG metabolism in mAO (Fig 1-B), neither does it exist for the dantrolene progress curves in either of

the species (Fig 1-C, D). Therefore, we used a linear Michaelis-Menten model to numerically fit the time course data in those plots. In the Michaelis-Menten model, k_3 represents the rate of product formation (k_{3_ox} for the 8-oxo-O6BG formation and k_{3_red} for ADNTN formation). Both of the substrates, O6BG, and dantrolene, were present at their saturating level (5 times the K_m or more) in the reaction to remove the possibility of substrate depletion. Therefore, the rates presented in Table 2 are representative of the maximum rate of reaction. Based on the comparison between the rate of product formation during each of the catalytic half-reactions under anaerobic conditions, there is almost a 166-fold difference between the oxidation rate (k_{3_ox}) from fitting the O6BG oxidation to MAM and the reduction rate (k_{3_red}) derived from fitting the dantrolene reduction to the Michaelis-Menten model in hAO. On the other hand, the k_{3_ox} is only 14-fold higher than the k_{3_red} in mAO. Also, despite the rate of oxidation (k_{3_ox}) in human being 50-fold faster than monkey, there is a much lower 4-fold difference in the rate of reduction (k_{3_red}) between the two species.

Probing the efficacy of reduction in AO under anaerobic conditions

To compare the efficacy of reduction between human and monkey, we have calculated the ratio of the concentration of the oxidized product (8-oxo-O6BG) to the concentration of the reduced product (ADNTN) formed during the enzymatic reaction and called this ratio OAR. AO performs nitro reduction on dantrolene and for a nitro group to be reduced, 6 electrons are required (Fig. 2A). In a perfect and hundred percent efficient case, the OAR ratio would be three since each round of O6BG oxidation provides two electrons out of the total of six electrons required to form ADNTN. The greater the electron leakage in the catalytic cycle is, the higher this ratio goes. An example of electron leakage could be a case of incomplete nitro reduction

leading to the release of hydroxylamine and nitroso-containing intermediates. A schematic presentation of the AO catalytic cycle and the electron flow pathway is demonstrated in Fig. 2B. Under anaerobic conditions and 5 times the K_m amount of O6BG and dantrolene, the OAR ratio is close to an average of 50.3 ± 20.7 in hAO while it holds a much closer to the ideal value of 3 (5.8 ± 1.8) for mAO (Table 3). This means that the efficacy of electron shuttle and reduction is almost 10-fold higher in mAO than hAO. It is also important to note that the efficacy of the electron shuttle or the balance between the enzymatic oxidation and reduction is the result of the combination of the binding affinity of the substrates as well as their rate of enzymatic turnover. We have performed all of the experiments using a saturating amount of each substrate to only compare the maximum rate of reaction in all cases.

Molecular basis of inter-species kinetic differences

To establish whether certain amino acids at the MoCo active site were responsible for the kinetic differences between hAO and mAO, we performed site-directed mutagenesis on hAO to make it more like mAO. Having as much as 95.1% sequence identity (Hoshino *et al.*, 2007) between hAO and mAO limits the number of amino acid differences to be considered to 58. We inspected the hAO crystal structure (PDB 4UHW) trying to pinpoint amino acid differences between human and cynomolgus monkey (hAO#mAO) close to the cofactors. We found that 6 of the differences are in the vicinity of the Mo site: K661E, V811A, L812F, I816V, F885L, and F1014Y. One further mutation, E274Q, is at the FAD domain at 8\AA from one of the FAD phosphates, being an exposed residue. We singled out the V811A and F885L out of only six MoCo-adjacent mutants as well as their double mutant (FLVA) for this investigation since the

phenylalanine and valine residues had been reported to play an important role in orienting the substrate at the MoCo site (Coelho *et al.*, 2015; Terao *et al.*, 2020).

Similar to what was observed for hAO and mAO, the dantrolene reduction progress curves under anaerobic conditions and with saturating amounts of O6BG and dantrolene remained linear with time for the mutants as well (Fig. 3). The initial visual assessment of the mutants' O6BG oxidation progress curves from the same reaction (Fig. 4) suggested a small shift towards a more linear monkey-like kinetic behavior. However, nonlinear kinetics were still observed for all the mutants, and based on the AIC criteria, the MAM gave a better fit to both F885L and V811A single mutants as well as their double mutant (FLVA) in comparison to the linear model (Fig. 4). We used the OAR criteria to assign human-like or monkey-like characteristics to all the mutated hAOs more quantitatively. At both ends of the spectrum stands hAO with an average OAR value of 50.3 ± 20.8 and mAO with an average OAR value of 5.83 ± 1.83 . Although all of the F885L, V811A, and FLVA mutants hold a lower average OAR value than hAO, 42.3 ± 18.2 , 31.0 ± 9.85 , and 32.8 ± 7.70 respectively, their OAR value was still much closer to human than that of the cynomolgus monkey.

Discussion:

AO has proven to be a challenging drug metabolizing enzyme for clearance estimation in humans. Not only is AO both substrate and species-specific, it also exhibits nonlinear atypical kinetics (Dalvie *et al.*, 2010; Barr *et al.*, 2013a; Choughule *et al.*, 2015; Abbasi *et al.*, 2019). With more than 95.1% sequence identity between human and cynomolgus monkey AO, cynomolgus monkey may be the best species to estimate AO clearance in human. The comparable AO-mediated metabolism of BIBX1382, SGX523, VU0409106, RS-8359, and zaleplon between human and cynomolgus monkey is also consistent with this notion (Kawashima *et al.*, 1999; Itoh *et al.*, 2006b; Diamond *et al.*, 2010; Garattini *et al.*, 2012; Morrison *et al.*, 2012; Hutzler *et al.*, 2013, 2014)

Our previous studies on numerous substrates of hAO have shown that this enzyme exhibits nonlinear, biphasic kinetics (Abbasi *et al.*, 2019). We have assigned the fast initial phase to the rate of substrate oxidation and the second slower phase to the stage during the enzymatic reaction where the enzyme re-oxidation is the rate-limiting step. Because the linear Michaelis-Menten model performs poorly with nonlinear data, we have modeled this biphasic kinetics using MAM (blue inset in Fig. 1-A). In this kinetic scheme, the fast initial phase is presented by the k_3 value and the slower phase is captured by the k_5 micro rate constant. What this means is that once all the hAO enzyme molecules in the reaction are reduced by the oxidizing substrates (e.g. O6BG), the reaction mostly proceeds at the rate of enzymatic re-oxidation (k_5) rather than the rate of substrate oxidation (k_{3_ox}). In contrast, linear kinetics was observed with mAO.

If the traditional method of determining the linear region of the progress curves is applied to derive the rate of the reaction, a significant amount of information that mechanistically differentiates hAO from mAO is lost. Herein we take the full time course into account to describe the differences in the AO metabolic progress curves for O6BG between monkey (linear) and human AO (nonlinear). This makes the comparison and identification of the molecular basis of their differences more feasible since rates are difficult to directly compare. Therefore, any structural differences between hAO, mAO, and their mutants mirrored in the progress curves would be visually easy to identify. Since there is a much smaller almost 14-fold difference between k_{3_ox} and k_{3_red} in mAO as opposed to a 166-fold difference in hAO, the linearity of the mAO progress curve can be attributed to a balance between the rate of the two catalytic half-reactions (Table 2). With the reduction as the rate-limiting step, there is a lower chance of electron backlog in mAO with a much slower oxidation rate in comparison to hAO. The same results were obtained with oxygen as the electron acceptor (Supplementary Table 1), eliminating the possibility of this kinetic discrepancy simply being the result of using a non-endogenous electron acceptor or having reductive intermediates.

Since both hAO and mAO have shown similar linear reductive kinetic behavior, we have decided to look into whether the interspecies kinetic differences can be explained by the differences in the oxidation binding site. The MoCo site of the human AO has been identified as the oxidative substrate's binding region. Therefore, we have first looked into the amino acid differences between the two species around this site. The two amino acids chosen for this study were the F885 and V811 residues which were identified as important amino acids in orienting

the substrate towards the catalytic site in human AO and stabilization of the intermediate MoCo species (Coelho *et al.*, 2015; Terao *et al.*, 2020).

The reduction is believed to be the rate-limiting step in AO catalytic cycle (Abbasi *et al.*, 2019). Therefore, a comparison between the k_{3_red} values in hAO and mAO as well as their mutants is of high importance (Table 2). While this value in F885L mutant remains the same as hAO, the V811A containing mutants seem to shift toward a more monkey-like, lower rate of reduction similar to mAO. However, since there is a catalytic cross-talk between the reduction and oxidation half-reactions, the nonlinearity of the progress curves in mutants is the result of an imbalance between k_{3_ox} and k_{3_red} similar to what was observed in hAO and this nonlinearity is not solely dependent to k_{3_red} .

In an attempt to quantitatively assess the differences between hAO, mAO, and their mutants, we have defined the OAR criteria as the stoichiometric ratio of [8-oxo-O6BG]/[ADNTN] made during the enzymatic reaction in the absence of oxygen. As shown in Figure 2, three oxidation reactions are required to fully reduce the nitro group in dantrolene to an amine. Experiments were done anaerobically to decrease the complexity of this analysis by removing an alternative electron acceptor (molecular oxygen) from the system. Therefore, a potential remaining pathway of electron leakage could be the formation of the reductive intermediates of dantrolene such as hydroxylamine and nitroso species. These intermediates could leave the reductive site before a complete nitro reduction into ADNTN occurs. While these compounds are reactive intermediates posing a risk of time-dependent inhibition (TDI) (Yadav *et al.*, 2020), there is no correlation between the biphasic kinetics for O6BG in hAO and TDI since such nonlinearity does not exist

for the reductive half-reaction for dantrolene in this enzyme (Fig. 3). In this sense, OAR could be used as the means to gauge the efficiency of electron shuttle from the oxidative site to the reductive site of the enzyme. The route that the electrons have to take is believed to be from the MoCo site to the FAD site and through the two iron-sulfur clusters that act as electron sinks during catalysis (Pryde *et al.*, 2010). Based on our results, OAR holds a much smaller value in cynomolgus monkey followed by V811A, FLVA, F885L, and human AO (Table 3). Overall, while we saw some progress towards more monkey-like kinetics in the mutants we explored (especially for the V811A containing mutants), other amino acids must also play a role in the kinetic differences between human and cynomolgus monkey AO.

Several other potentially important amino acid differences, especially the K661E at the gate 1 of the substrate access channel, as well as L812F which is another important amino acid difference pointing to the entrance of the active site pocket still remain to be considered at the MoCo site of AO (Coelho *et al.*, 2015). However, recent publications regarding the AO nitro reduction, most notably the one by Paragas *et al.* in which the FAD site has been suggested as the reductive site of this enzyme, has brought up the possibility of amino acids at this site also having an important role in causing this marked kinetic difference between the two species (Konishi *et al.*, 2017; Paragas *et al.*, 2017a; Amano *et al.*, 2018; Ogiso *et al.*, 2018). However, it is also important to note that there are two sites involved in playing this catalytic see-saw. Therefore, there is always the possibility of requiring a change in a combination of amino acids at both of the FAD and MoCo sites in hAO to arrive at a kinetic behavior that is more similar to mAO.

In conclusion, while hAO and mAO share a high degree of sequence similarity, they do not share common kinetics, and mAO may not be a good model for hAO. Attempts to understand why hAO and mAO are different, using site-directed mutagenesis of amino acid in the MoCo active-site showed some progress towards slower monkey-like kinetics especially in the V811A containing mutants. However, we believe that differences in the structure outside the MoCo active-site may also be responsible for the differences in kinetics.

Acknowledgments

We thank Dr. Sara Humphreys for her help in proof-reading this manuscript and her insightful comments.

Authorship Contributions

Participation in research design: Abbasi, and Jones.

Conducted experiments: Abbasi, and Joswig-Jones.

Performed data analysis: Abbasi, and Jones.

Wrote or contributed to the writing of the manuscript: Abbasi, and Jones.

References:

- Abbasi A, Paragas EM, Joswig-Jones CA, Rodgers JT, and Jones JP (2019) The Time-course of Aldehyde Oxidase and the Reason Why it is Nonlinear. *Drug Metab Dispos* **47**:dmd.118.085787, American Society for Pharmacology and Experimental Therapy.
- Alfaro JF, and Jones JP (2008) Studies on the mechanism of aldehyde oxidase and xanthine oxidase. *J Org Chem* **73**:9469–9472.
- Alfaro JF, Joswig-Jones CA, Ouyang W, Nichols J, Crouch GJ, and Jones JP (2009) Purification and Mechanism of Human Aldehyde Oxidase Expressed in. *Pharmacology* **37**:2393–2398.
- Amano T, Fukami T, Ogiso T, Hirose D, Jones JP, Taniguchi T, and Nakajima M (2018) Identification of enzymes responsible for dantrolene metabolism in the human liver: A clue to uncover the cause of liver injury. *Biochem Pharmacol* **151**:69–78, Elsevier.
- Barr JT, and Jones JP (2013a) Evidence for substrate-dependent inhibition profiles for human liver aldehyde oxidase. *Drug Metab Dispos* **41**:24–29.
- Barr JT, Jones JP, Joswig-Jones CA, and Rock DA (2013b) Absolute quantification of aldehyde oxidase protein in human liver using liquid chromatography-tandem mass spectrometry. *Mol Pharm* **10**:3842–3849.
- Cheshmazar N, Dastmalchi S, Terao M, Garattini E, and Hamzeh-Mivehroud M (2019) Aldehyde oxidase at the crossroad of metabolism and preclinical screening. *Drug Metab Rev*, doi: 10.1080/03602532.2019.1667379.
- Choughule K V., Barr JT, and Jones JP (2013) Evaluation of rhesus monkey and guinea pig hepatic cytosol fractions as models for human aldehyde oxidase. *Drug Metab Dispos* **41**:1852–1858.

- Choughule K V., Joswig-Jones CA, and Jones JP (2015) Interspecies differences in the metabolism of methotrexate: An insight into the active site differences between human and rabbit aldehyde oxidase. *Biochem Pharmacol* **96**:288–295, Elsevier Inc.
- Coelho C, Foti A, Hartmann T, Santos-Silva T, Leimkühler S, and Romão MJ (2015) Structural insights into xenobiotic and inhibitor binding to human aldehyde oxidase. *Nat Chem Biol* **11**:779–783.
- Crouch RD, Hutzler JM, and Daniels JS (2018) A novel in vitro allometric scaling methodology for aldehyde oxidase substrates to enable selection of appropriate species for traditional allometry. *Xenobiotica* **48**:219–231, Informa UK Limited, trading as Taylor & Francis Group.
- Dalvie D, Xiang C, Kang P, and Zhou S (2013) Interspecies variation in the metabolism of zoniporide by aldehyde oxidase. *Xenobiotica* **43**:399–408.
- Dalvie D, Zhang C, Chen W, Smolarek T, Obach RS, and Loi CM (2010) Cross-species comparison of the metabolism and excretion of zoniporide: Contribution of aldehyde oxidase to interspecies differences. *Drug Metab Dispos* **38**:641–654.
- Davydova NY, Dangi B, Maldonado MA, Vavilov NE, Zgoda VG, and Davydov DR (2019) Toward a systems approach to cytochrome P450 ensemble: Interactions of CYP2E1 with other P450 species and their impact on CYP1A2. *Biochem J* **476**:3661–3685.
- Diamond S, Boer J, Maduskuie TP, Falahatpisheh N, Li Y, and Yeleswaram S (2010) Species-specific metabolism of SGX523 by aldehyde oxidase and the toxicological implications. *Drug Metab Dispos* **38**:1277–1285.
- Dittrich C, Greim G, Borner M, Weigang-Köhler K, Huisman H, Amelsberg A, Ehret A, Wanders J, Hanauske A, and Fumoleau P (2002) Phase I and pharmacokinetic study of

- BIBX 1382 BS, an epidermal growth factor receptor (EGFR) inhibitor, given in a continuous daily oral administration. *Eur J Cancer* **38**:1072–80.
- Dowers TS, Rock Dan A., Rock Denise A., Perkins BNS, and Jones JP (2004) An analysis, of the regioselectivity of aromatic hydroxylation and N-oxygenation by cytochrome P450 enzymes. *Drug Metab Dispos* **32**:328–332.
- Foti A, Hartmann T, Coelho C, Santos-Silva T, Romão MJ, and Leimkühler S (2016) Optimization of the expression of human aldehyde oxidase for investigations of single-nucleotide polymorphisms. *Drug Metab Dispos* **44**:1277–1285.
- Fukiya K, Itoh K, Yamaguchi S, Kishiba A, Adachi M, Watanabe N, and Tanaka Y (2010) A single amino acid substitution confers high cinchonidine oxidation activity comparable with that of rabbit to monkey aldehyde oxidase 1. *Drug Metab Dispos* **38**:302–307.
- Garattini E, Fratelli M, and Terao M (2009) The mammalian aldehyde oxidase gene family. *Hum Genomics* **4**:119–130.
- Garattini E, and Terao M (2012) The role of aldehyde oxidase in drug metabolism.
- Hoshino K, Itoh K, Masubuchi A, Adachi M, Asakawa T, Watanabe N, Kosaka T, and Tanaka Y (2007) Cloning, expression, and characterization of male cynomolgus monkey liver aldehyde oxidase. *Biol Pharm Bull* **30**:1191–1198.
- Hutzler JM, Cerny MA, Yang YS, Asher C, Wong D, Frederick K, Gilpin K, Sugihara K, Katsuma Y, Kitamura S, Ohta S, Fujitani M, and Shintani H (2014) Cynomolgus monkey as a surrogate for human aldehyde oxidase metabolism of the EGFR Inhibitor BIBX1382. *Drug Metab Dispos* **42**:1751–1760.
- Hutzler JM, Obach RS, Dalvie D, and Zientek MA (2013) Strategies for a comprehensive understanding of metabolism by aldehyde oxidase. *Expert Opin Drug Metab Toxicol* **9**:153–

168.

Itoh K, Hoshino K, Endo A, Asakawa T, Yamakami K, Noji C, Kosaka T, and Tanaka Y (2006a)

Chiral inversion of RS-8359: A selective and reversible MAO-A inhibitor via oxidation-reduction of keto-alcohol. *Chirality* **18**:698–706.

Itoh K, Yamamura M, Takasaki W, Sasaki T, Masubuchi A, and Tanaka Y (2006b) Species

differences in enantioselective 2-oxidations of RS-8359, a selective and reversible MAO-A inhibitor, and cinchona alkaloids by aldehyde oxidase. *Biopharm Drug Dispos* **27**:133–139.

Kawashima K, Hosoi K, Naruke T, Shiba T, Kitamura M, and Watabe T (1999) Aldehyde

oxidase-dependent marked species difference in hepatic metabolism of the sedative-hypnotic, zaleplon, between monkeys and rats. *Drug Metab Dispos* **27**:422–8.

Konishi K, Fukami T, Gotoh S, and Nakajima M (2017) Identification of enzymes responsible

for nitrazepam metabolism and toxicity in human. *Biochem Pharmacol* **140**:150–160, Elsevier Inc.

Li H, Kundu TK, and Zweier JL (2009) Characterization of the magnitude and mechanism of

aldehyde oxidase-mediated nitric oxide production from nitrite. *J Biol Chem*, doi: 10.1074/jbc.M109.019125.

Maia LB, Pereira V, Mira L, and Moura JJG (2015) Nitrite reductase activity of rat and human

xanthine oxidase, xanthine dehydrogenase, and aldehyde oxidase: Evaluation of their contribution to NO formation in vivo. *Biochemistry*, doi: 10.1021/bi500987w.

Mendel RR (2009) Cell biology of molybdenum. *BioFactors* **35**:429–434.

Morrison RD, Blobaum AL, Byers FW, Santomango TS, Bridges TM, Stec D, Brewer KA,

Sanchez-Ponce R, Corlew MM, Rush R, Felts AS, Manka J, Bates BS, Venable DF,

Rodriguez AL, Jones CK, Niswender CM, Conn PJ, Lindsley CW, Emmitte KA, and

- Daniels JS (2012) The role of aldehyde oxidase and xanthine oxidase in the biotransformation of a novel negative allosteric modulator of metabotropic glutamate receptor subtype 5. *Drug Metab Dispos* **40**:1834–1845.
- Mota C, Esmaeeli M, Coelho C, Santos-Silva T, Wolff M, Foti A, Leimkühler S, and Romão MJ (2019) Human aldehyde oxidase (hAOX1): structure determination of the Moco-free form of the natural variant G1269R and biophysical studies of single nucleotide polymorphisms. *FEBS Open Bio* **9**:925–934.
- Nair A, and Jacob S (2016) A simple practice guide for dose conversion between animals and human. *J Basic Clin Pharm* **7**:27.
- Ogiso T, Fukami T, Mishiro K, Konishi K, Jones JP, and Nakajima M (2018) Substrate selectivity of human aldehyde oxidase 1 in reduction of nitroaromatic drugs. *Arch Biochem Biophys* **659**:85–92, Academic Press Inc.
- Paragas EM, Humphreys SC, Min J, Joswig-Jones CA, and Jones JP (2017a) The two faces of aldehyde oxidase: Oxidative and reductive transformations of 5-nitroquinoline. *Biochem Pharmacol* **145**:210–217, Elsevier Inc.
- Paragas EM, Humphreys SC, Min J, Joswig-Jones CA, Leimkühler S, and Jones JP (2017b) ecoAO: A Simple System for the Study of Human Aldehyde Oxidases Role in Drug Metabolism. *ACS Omega* **2**:4820–4827, American Chemical Society.
- Pryde DC, Dalvie D, Hu Q, Jones P, Obach RS, and Tran T-D (2010) Aldehyde Oxidase: An Enzyme of Emerging Importance in Drug Discovery. *J Med Chem* **53**:8441–8460.
- Sharma V, and McNeill JH (2009) To scale or not to scale: The principles of dose extrapolation. *Br J Pharmacol* **157**:907–921.
- Terao M, Garattini E, Romão MJ, and Leimkühler S (2020) Evolution, expression, and substrate

specificities of aldehyde oxidase enzymes in eukaryotes. *J Biol Chem* jbc.REV119.007741.

Weidert ER, Schoenborn SO, Cantu-Medellin N, Jones JP, and Kelley EE (2013) Inhibition of Xanthine Oxidase by the Aldehyde Oxidase Inhibitor Raloxifene: Implications for Identifying Molybdopterin Nitrite Reductases. *Free Radic Biol Med*, doi: 10.1016/j.freeradbiomed.2013.10.638.

Yadav J, Paragas E, Korzekwa K, and Nagar S (2020) Time-dependent enzyme inactivation: Numerical analyses of in vitro data and prediction of drug-drug interactions. *Pharmacol Ther* **206**:107449.

Zhang X, Liu HH, Weller P, Zheng M, Tao W, Wang J, Liao G, Monshouwer M, and Peltz G (2011) In silico and in vitro pharmacogenetics: Aldehyde oxidase rapidly metabolizes a p38 kinase inhibitor. *Pharmacogenomics J* **11**:15–24.

Zhao SX, Forman D, Wallace N, Smith BJ, Meyer D, Kazolias D, Gao F, Soglia J, Cole M, and Nettleton D (2005) Simple strategies for reducing sample loads in in vitro metabolic stability high-throughput screening experiments: A comparison between traditional, two-time-point and pooled sample analyses. *J Pharm Sci*, doi: 10.1002/jps.20213.

Zientek M, Jiang Y, Youdim K, and Obach RS (2010) In vitro-in vivo correlation for intrinsic clearance for drugs metabolized by human aldehyde oxidase. *Drug Metab Dispos* **38**:1322–1327.

Footnotes

This work was supported by the National Institute of General Medical Sciences [GM100874].

Figure Legends

Figure 1. The time course plot of the product formation under anaerobic conditions using glucose oxidase to remove oxygen (as described in materials and methods) is presented for A) O6BG in **hAO** B) O6BG in **mAO**, C) dantrolene in **hAO** and D) dantrolene in **mAO**. Saturating concentration (5 times the K_m) of both oxidative (O6BG, 200 μM) and reductive (dantrolene, 30 μM) substrates were used for these kinetic assays. The kinetic models used in fitting these datasets are presented as blue insets and the R-squared values are mentioned on the bottom right side of each graph. The Modified Activity model (MAM) was used for A and the Michaelis-Menten linear model was used for B, C, and D. Models were selected according to the kinetic trend of the product formation in each dataset.

Figure 2. A) The nitro-reduction pathway: for a full nitro-reduction to happen, 6 electrons are required but nitroso and hydroxylamine intermediates could also be formed during this process. B) A schematic presentation of the anaerobic AO catalytic cycle for O6BG as the oxidative substrate and dantrolene as the reductive substrate. The electron flow pathway from the MoCo site to the FAD site through the two iron-sulfur clusters is presented with a dashed arrow. The electron leakage through nitroso and hydroxylamine intermediates formed as a result of incomplete nitro-reduction can pose a risk of time-dependent inhibition (TDI) of the enzyme (orange dotted arrow). However, this is not the case for O6BG oxidation by AO.

Figure 3. The time course plot of the ADNTN formation under anaerobic conditions using a saturating amount of O6BG (200 μM) as the oxidative substrate and dantrolene as the reductive substrate (30 μM). A glucose oxidase system was used to remove oxygen (as described in the

materials and methods) in all of the anaerobic reactions. The reductive half-reaction remained linear and was fit to the Michaelis-Menten model in all the mutants, F885L (black, $R^2= 0.98$), V811A (magenta, $R^2= 0.95$), and FLVA (purple, $R^2= 0.96$), similar to **hAO** (red, $R^2= 0.98$) and **mAO** (blue, $R^2= 0.91$).

Figure 4. The time course plot of 8-oxo-O6BG formation by A) **hAO**, B) **mAO**, C) F885L, D) V811A and E) FLVA double mutant under anaerobic conditions using saturating concentration of O6BG (200 μ M) and dantrolene (30 μ M) is presented here. The data for all the enzymatic reactions were fit to the MAM except for **mAO** for which the linear Michaelis-Menten model was used.

Table 1. The human to monkey (**hAO#mAO**) mutants were made using the primers, DNA templates, and the sequencing primers as described.

Plasmid (hAO#mAO)	Primer	DNA Template	Sequencing Primer
F885L	FW: 5'-cagaccattcaataactaacaggctttcatccagg-3' RV: 5'-cctggatgaaagcctgttagttattgaaatgggtctg-3'	pTHco-AOX1	5'-attgtgccagcactgaa-3' (Nucleotides 2401--2800)
V811A	FW: 5'-aataataccggtttcagcgctttaccaccaaatgcacc-3' RV: 5'-ggtgcatttggtgtaaaagcgtgaaaaccggtattatt-3'	pTHco-AOX1	
FLVA	FW: 5'-aataataccggtttcagcgctttaccaccaaatgcacc-3' RV: 5'-ggtgcatttggtgtaaaagcgtgaaaaccggtattatt-3'	F885L	

Table 2. A comparison between the rate of product formation between the two species as well as the mutants under anaerobic conditions using a glucose oxidase system as described in the methods section. MAM was the model of choice in fitting the O6BG (200 μ M) product formation for **hAO** and all the mutants and Michaelis-Menten linear model was used to fit the O6BG product formation in **mAO** as well as the product formation for dantrolene (30 μ M) in both species and the mutants.

	rate of 8-oxo-O6BG formation, min ⁻¹			rate of ADNTN formation, min ⁻¹
	k _{3_ox}	k ₄	k ₅	k _{3_red}
hAO	110± 20.7	0.160± 0.0494	9.28± 2.03	0.659± 0.0182
mAO	2.19± 0.0696	---	---	0.156± 0.00876
F885L	38.7± 3.85	0.0388± 0.0144	7.90± 2.71	0.701± 0.0193
V811A	40.7± 8.51	0.158± 0.0486	2.95± 0.522	0.336± 0.0143
FLVA	30.4± 5.02	0.0659± 0.0289	7.50± 1.37	0.486± 0.0199

Table 3. The change in the ratio of the concentration of the oxidative to reductive product (OAR) with time under anaerobic conditions (as described in the methods section) and saturating amount of the oxidative and reductive substrates, O6BG (200 μ M) and dantrolene (30 μ M) respectively.

Time, minutes	[8-oxo-O6BG]/[ADNTN], μ M/ μ M				
	hAO	mAO	F885L	V811A	FLVA
0.2	55.6 \pm 19.3	4.41 \pm 0.622	86.0 \pm 42.2	46.1 \pm 23.9	21.7 \pm 4.54
3	71.8 \pm 26.8	3.59 \pm 1.38	39.8 \pm 8.20	34.4 \pm 9.70	28.8 \pm 1.54
10	71.3 \pm 16.9	4.43 \pm 1.32	42.1 \pm 7.22	39.8 \pm 8.45	39.5 \pm 2.71
20	61.0 \pm 12.0	5.99 \pm 0.881	47.2 \pm 2.31	37.4 \pm 8.09	40.3 \pm 2.51
30	52.7 \pm 5.68	5.41 \pm 1.48	43.4 \pm 1.34	33.8 \pm 4.41	40.6 \pm 3.53
45	39.3 \pm 8.13	6.78 \pm 1.64	38.6 \pm 3.67	27.7 \pm 2.54	38.1 \pm 5.25
60	33.5 \pm 5.94	7.63 \pm 1.72	34.6 \pm 3.24	23.9 \pm 1.79	34.8 \pm 6.57
90	25.3 \pm 3.30	7.90 \pm 1.60	26.7 \pm 2.40	19.5 \pm 1.09	29.5 \pm 4.25
120	20.6 \pm 2.57	8.53 \pm 2.62	22.3 \pm 2.71	16.3 \pm 0.875	21.4 \pm 0.972
Average	50.3\pm 20.8	5.83\pm 1.83	42.3\pm 18.2	31.0\pm 9.85	32.8\pm7.70

Figure 1.

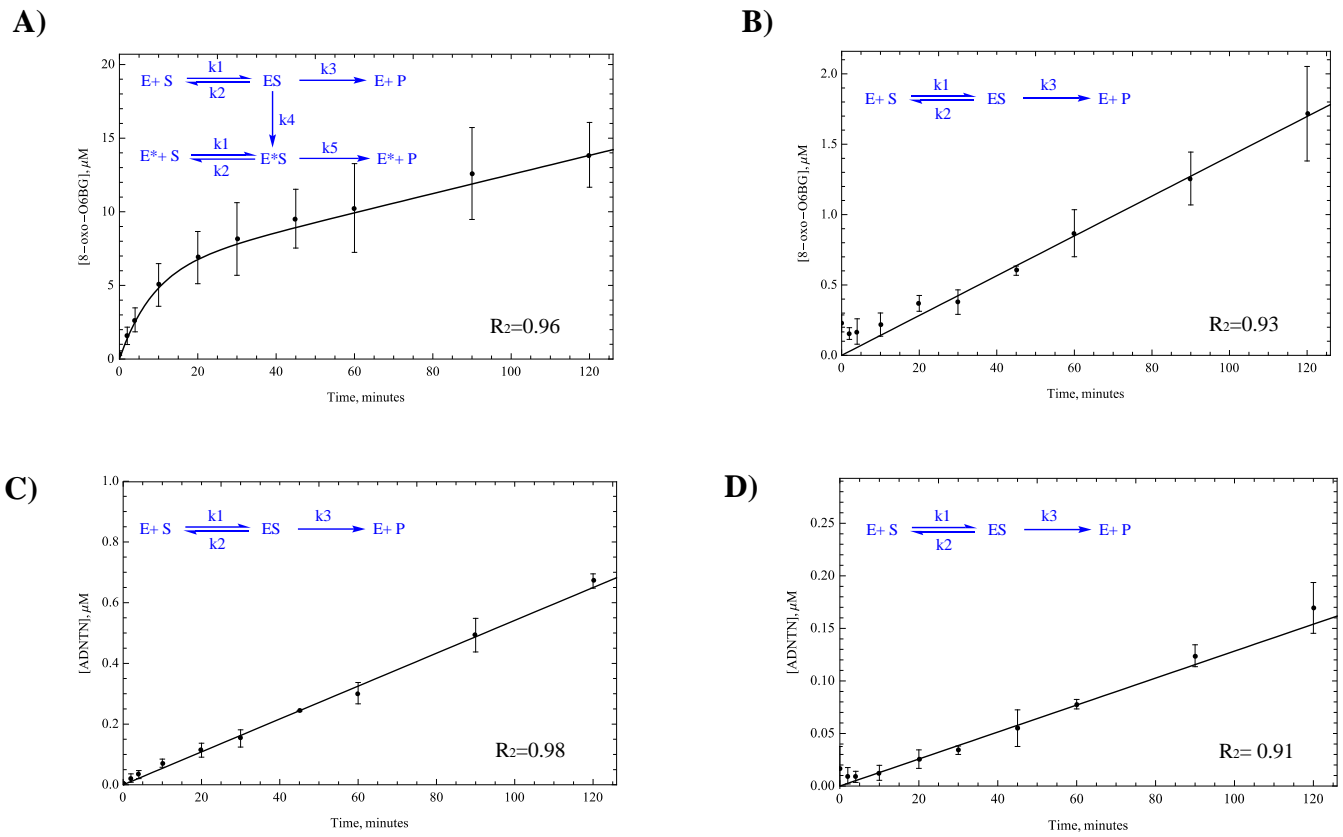


Figure 2.

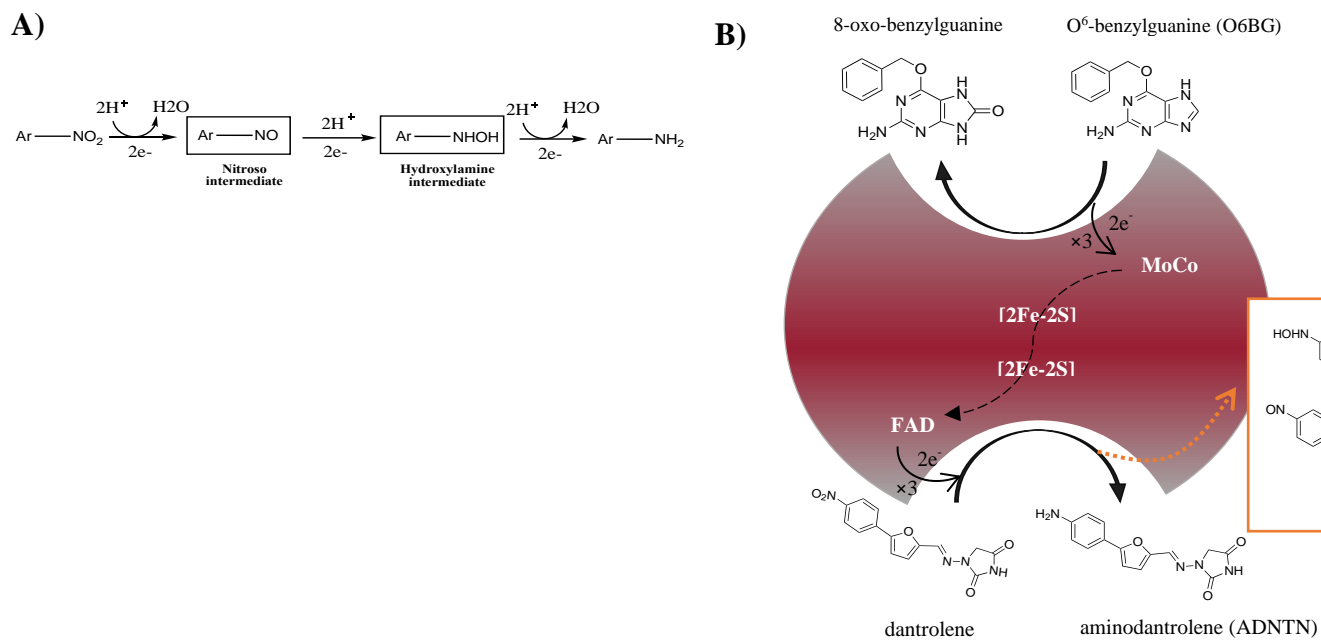


Figure 3.

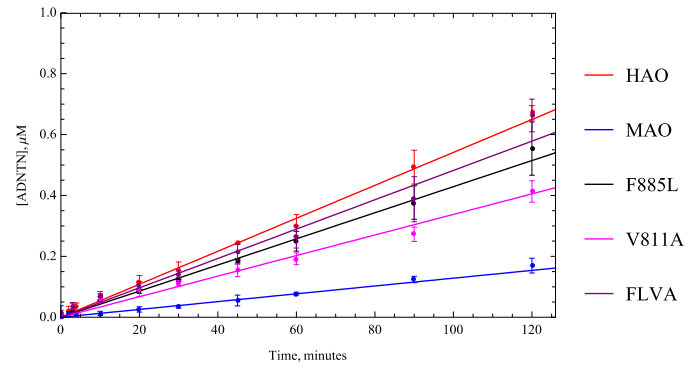


Figure 4.

